Enhanced Photocatalytic Performance of Nb Doped TiO2/reduced Graphene Oxide Nanocomposites Over Rhodamine B Dye Under Visible Light Illumination

N. Prabhakarrao
Andhra University College of Science and Technology
K.V. Divya Lakshmi
Andhra University College of Science and Technology
G. Divya
Andhra University College of Science and Technology
G. Jaishree
Andhra University College of Science and Technology
Imandi Manga Raju
Andhra University College of Science and Technology
Shaik Abdul Alim
Andhra University College of Science and Technology
Siva Rao Tirukkovalluri (sivaraoau@gmail.com)
Andhra University https://orcid.org/0000-0001-5156-1885

Research

Keywords: Graphene oxide, Niobium, Photocatalysis, Rhodamine B dye, Titanium oxide

Posted Date: March 5th, 2021

DOI: https://doi.org/10.21203/rs.3.rs-275142/v1

Version of Record: A version of this preprint was published at Sustainable Environment Research on November 20th, 2021. See the published version at https://doi.org/10.1186/s42834-021-00110-x.

Abstract

The present study discusses the synthesis of Nb doped TiO_2/reduced Graphene Oxide (GO) intercalated nanocomposites *via* sol-gel route at a lower temperature by using different loading amounts of GO (1 to 10 wt%). The synthesized composite materials were further characterized by copious instruments such as X-ray Diffractometer, UV-vis Diffuse Reflectance Spectroscopy, Scanning Electron Microscopy, Transmission Electron Microscopy, BET surface area analysis, Raman and FT-Infrared Spectroscopy. The experimental results stated that the Nb doped TiO_2 nanoparticles uniformly distributed on the surface of reduced Graphene Oxide (rGO) with an interfacial linking bond between TiO_2 and rGO. Later, the photocatalytic degradation of Rhodamine B dye using produced materials under visible light irradiations was examined. These results reveal that Nb doped TiO_2/rGO nanocomposites exhibited better photocatalytic performance than Nb doped TiO_2 for the removal of Rhodamine B dye. However, among all, the nanocomposite having 5% of GO content achieves the highest degradation rate for Rhodamine B dye approximately 98% under visible light exposure. Overall, the unique properties such as electron accepting and transporting properties of GO in the nanocomposites help to enhance photocatalytic activity by minimizing the charge carrier's recombination rate.

1. Introduction

Since the past few decades, textile wet processing and finishing industries are strongly dependent on synthetic dyes that severely contaminating water along with other very harmful organic pollutants. Cleansing of industrial wastewater is attracting more importance in present days due to toxic, low biodegradable, high persistence and carcinogenic nature of dye pollutants. Removal of these complex dye molecules is compulsory before their emergence into the environmental streams [1, 2]. These are degraded naturally under alkaline conditions, ultraviolet (UV) light illumination, high temperature, and other radical initiators. Unfortunately, by-products from these processes are more hazards than original dyes to the environment [3]. Thus, for removing dyes from textile wastewater, an effective and economical treatment technique is needed. In view of this, various conventional methods have been developed to remove these most harmful and complex structured dye molecules from waste water such as adsorption on carbon materials, coagulation, flocculation, reverse osmosis (RO), biodegradation, membrane filtration, ozonation, advanced oxidation process (AOP) etc [4, 5]. Among these, AOP is largely adopted method for remediation of dye contaminated effluents because of their flexibility, efficacy and relatively low expensive [6]. AOP covers wide variety of treatment techniques; among those approaches, semiconductor-mediated photocatalytic oxidation has been used extensively to abolish the recalcitrant organic pollutants from its contaminated wastewater. With this process degradation of a broad array of organic pollutants is possible which finally turns into H_2O, CO_2, etc through oxidation-reduction interactions between organic pollutants with photogenerated reactive oxygen species [7].

In particular, Titania (TiO_2) has been generally admitted as a promising photocatalyst for the decomposition of hazardous environmental impurities owing to its unique physical and chemical

properties [8]. However, due to large band gap energy 3.2 eV (anatase TiO_2) and poor electron mobility, it shows very limited photosensitization in the visible range of Earth's solar spectrum. To overcome the grand challenges, several efforts have been made by researchers such as transition and noble metals doping [9, 10], semiconductors coupling [11], surface polymer sensitization [12, 13] and combination with carbonaceous materials [14]. In particular, metal ion doping of TiO_2 along with carbonaceous material combination is the emerging area at present in the photocatalysis. Doping can narrow the band gap and carbonaceous material can limit the charge carriers (e^- - h^+ pair) recombination [15]. There are several investigators reported doping of TiO_2 lattice with numerous transition metal ions i.e., Cr, Cu, Zr, Ce, Sn, Fe, Ni etc [16]. Presently, as compare with many dopants, Nb doped TiO_2 has attracted greater attention because of its utilization in various applications like photocatalysis, dye sensitized solar cells, sensors, fuel cell catalysis, and transparent conductive films [16]. It is mainly due to the ionic radius of Nb^{5+} (0.064 nm) is significantly larger than Ti^{4+} (0.0605 nm) which effectively constricts the band gap of TiO_2 to enlarge its adsorption in visible region and on the other side metals are thermally unstable as well as effortless to cause the charge carriers recombination [17].

Given on this obstacle, several researchers investigated and achieved efficient photocatalyst by providing 2-Dimensional support to TiO_2 nanoparticles such as multiwall carbon nanotubes because of its multiple grapheme layers contacts with TiO_2 allows electrons can flow through, which accelerate the photogenerated charge separation more favorably [18]. Significant results have been obtained using graphene as 2-dimensional supporting material to catalyst due to that this material has a single atomic thick two-dimensional hexagonal lattice sheet structure aligned by a sp^2-hybridized carbon network and its wide variety of features such as electrical, thermal, mechanical, etc [19]. Additionally, the surface of graphene can be easily fabricated with different functional groups in contrast to carbon nanotubes. It is a 0 eV bandgap semiconductor [20] with high charge carrying property [21], high specific area (2600 m^2g^{-1}) [22], high adsorption capacity and can be produced efficiently through "graphite oxide" intermediate from inexpensive natural graphite [23]. Because of the hydrophobic nature of graphene, strong intercalation of metal oxide on graphene surface is difficult. In spite of this, chemically modified graphene-based materials like Graphene Oxide (GO) and reduced Graphene Oxide (rGO) drawing more attention in semiconductor photocatalysis as supporting material. The existing oxygen functionalities in GO and rGO, like carbonyl (C = O), hydroxyl (O-H), epoxide (C-O-C) groups making graphene to display wonderful hydrophilic character and good intercalation chemistry [24]. It appears reasonable to conceive that much greater advancement in photocatalytic performance of Nb doped TiO_2 (NT) can be achieved by the novel Nb doped TiO_2/rGO composite materials with high interfacial contact and potential.

Herein, this paper demonstrated that synthesis of Nb-doped TiO_2/rGO (NTG) nanocomposite by altering the GO loads using a modified sol-gel method via *in situ* process at low temperature, which is industrially scalable. Improvement in the photocatalytic efficiency of NTG catalysts caused by GO insertion was orderly investigated depending upon the electronic structure, optical absorption, microstructure, and

electrochemical behaviours. The photocatalytic activity of the NTG nanocomposites was assayed by degrading the Rhodamine B (RhB) under visible light exposure.

RhB is a Xanthene group dye that is broadly using as a colouring compound in the manufacturing industries such as textiles, food products, paper, pharmaceutical, and dye laser production. Besides, also used for visual identification to illustrate the rate, flow path, and movement within water. As a consequence, it has been confirmed that polluted water with Rhodamine dyes could cause subcutaneous tissue borne sarcoma which is extremely fatal. Furthermore, other types of toxicities like reproductive and neurotoxicity have been thoroughly and intensively inspected as well as verified by the exposure of these dyes [25].

2. Materials And Methods

2.1. Chemical reagents

Reagents included Titanium tetra n-butoxide (TTBO) (E-Merck, Germany) and Niobium Chloride ($NbCl_5$) (Koch-light laboratories ltd.) were taken as Ti and Nb sources respectively for the preparation of nanocomposites. Sodium nitrate ($NaNO_3$), potassium permanganate ($KMnO_4$), 36.0–38.0% of hydrochloric acid (HCl) and 95.0–98.0% of sulphuric acid (H_2SO_4), ethanol and hydrogen peroxide (H_2O_2) were obtained from E-Merck (India). Graphite (99%) flakes purchased from Sigma Aldrich, USA and used for the synthesis of GO. To perform the photocatalytic degradation experiment, aqueous RhB dye (HI-Media, India) solution was used. For solutions preparation, doubly distilled water was used. All these specified chemicals were analytical grade reagents used without further purification.

2.2. Synthesis of Graphene Oxide

The modified hummer's method was adopted to synthesize GO by the oxidation process under acidic conditions [26]. Briefly, graphite powder (1.0 g) and $NaNO_3$ (0.5 g) were added together into Con. H_2SO_4 (23 mL). Then, $KMnO_4$ (3.0 g) was added simultaneously with vigorous stirring in cold condition and the reaction mixture temperature was regulated in an ice bath below 20 ^{0}C. Further, the reaction mixture was stirred for 30 min at 35 ^{0}C. Followed by the slow addition of 46 mL of distilled water causes in raising the temperature to 100 ^{0}C and continued stirring for 15 min, then the reaction was abolished by the addition of distilled water and H_2O_2 (30%) solution. Then, the suspension was centrifuged and obtained GO was washed thoroughly with 5% HCl solution and distilled water periodically until got confirmation of sulphate anion (SO_4^{-2}) absence. The resultant GO was dried at 50 ^{0}C.

2.3. Nb doped TiO_2/rGO nanocomposite synthesis

Following the previously reported method by same author [27] NTG composites were synthesized via *in situ* process through modified sol-gel approach by dispersing different GO concentrations from 1 to 10% weight ratios and fixing Nb loading as 5 wt% corresponding to Ti from previous studies [28] at low temperatures and schematic representation of synthesis process shown in Fig. 1. Partial deoxygenating

of GO to rGO and the deposition of NT on the surface of rGO occurred simultaneously during the synthesis process. Also, an excellent interfacial contact can be achieved between NT and rGO sheets through this synthesis process. In a typical synthesis route, $NbCl_5$ and TTBO have chosen as source materials for Nb and Ti respectively. Firstly, 0.305 g of Nb (5 wt%) was added into 50 mL of Ethanol solution stirred for 30 min and then 15 mL TTBO was mixed simultaneously and resultant noted as solution I. Next, 0.021 g of GO taking into 50 mL of ethanol (containing 1 wt% of GO relevant to Ti) underwent ultrasonication for 1 h to obtain homogeneous GO suspension named as Solution II. These following two solutions mixed vigorously by adding solution I into solution II slowly. Followed by the addition of 2 mL water and 1 mL nitric acid mixture (H_2O: HNO_3 = 2: 1 ratio) dropwise through the burette to attain solution mixture under continuous stirring. The obtained colloidal suspension was undergone for more than 1 h stirring and was aged at 25 ^{0}C until gel formation has occurred. The resulting wet gel was dried at 70 ^{0}C in a hot air oven for 24 h and ground; the resultant powder labelled as NTG1. By following the same procedure NTG5, NTG10 and NT were synthesized by varying the GO concentrations in colloidal suspension from 5% GO, 10% GO and without GO respectively.

2.4. Characterization techniques

The structural characteristics of as-synthesized materials were studied by analytical X-ray diffractometer (XRD) at room temperature using Cu Kα radiation operated at 30.0 kV and 30.0 mA over at 2^0 per min scan rate. The optical properties investigation of as-prepared samples was carried out by using $BaSO_4$ as reference material over the spectral range of 200–800 nm on a UV-visible diffuse reflectance spectrophotometer (DRS) (Scinco Co. Ltd., S-3100). The morphologies of photocatalysts can be ascribed on scanning electron microscopy (SEM) (JSM-6610 LV) which was outfitted with an energy dispersive X-ray analysis system (EDX). The TEM analysis of NTG nanocomposites was examined on a JEOL 120 KV transmission electron microscopy (TEM) instrument with copper grid support. The surface areas and pore size distribution of the nanocomposites were described from nitrogen adsorption–desorption isotherms calculations which are recorded on Brunauer-Emmett-Teller (BET) (Quantachrome Nova version 10.0) at -196 ^{0}C. Chemical states of constituent elements in the as-synthesized NTG5 sample were studied with X-ray photoelectron spectroscopy (XPS) (PHI quantum ESCA microprobe system) using the AlKα line of a 250-W X-ray tube as a radiation source with an energy of 12,536 eV, current of 16 mA and voltage of 12.5 kV. Raman measurements are noted by using the RM2000 Raman spectrometer. Fourier Transform Infra-Red (FT-IR) spectra were obtained on Shimadzu FT-TR spectrophotometer over the frequency range of 400–4000 cm^{-1} with KBr pellets as a reference sample to explain surface functionalities of photocatalysts. The decomposition kinetics for the photocatalytic activity of nanocomposites was acquired on a UV-visible spectrophotometer (UV-2200, Shimadzu, Japan). By using a fluorescence spectrophotometer (Hitachi, F-7000, Japan), photoluminescence (PL) spectra were obtained; the instrument was operated at 315 nm excitation wavelength with the 1200 nm/min scan rate followed by 700 V PMT voltage at room temperature. The slit width of both excitation and emission was 5.0 nm.

2.5. Experimental procedure for the photocatalytic activity of nanocomposites

Photocatalytic decomposition capabilities of NTG catalysts were evaluated under visible light stimulation by the degradation of choice pollutant RhB in aqueous solution. Photodecomposition experiments of RhB dye were performed in a photo reactor which consists of 400 W mercury high-pressure vapor lamp using as visible light source with oriel (51472) cut-off filter to remove undesired UV-radiation and placed it about 20 cm distance far from the reaction vessel. The running water system was circulated around the reaction vessel to maintain the reaction system at room temperatures and also to exclude IR radiation.

The experimental procedure as follows, initially 0.050 g catalyst (NT and NTG nanocomposites) was dispersed in 100.0 mL (2 mg/L) of RhB aqueous solution. After stirring under dark condition for 30 min to attain adsorption-desorption equilibrium, the light was switched on for testing. A sample of 5.0 mL well-dispersed suspension containing photocatalyst particles was withdrawn by a Millipore syringe at regular intervals of time and the photocatalyst particles were separated by centrifugation from collected suspension prior to analysis. The change in RhB dye concentration was measured by absorbance at 543 nm using a UV-visible spectrophotometer.

The extent of photodegradation efficiency of catalysts was calculated by obtaining the relationship between C/C_0 and illumination time (min), here C and C_0 are the concentrations of RhB dye at time t and time zero respectively. Because the RhB concentration changes (C/C_0) were directly proportional to absorbance changes (A/A_0) during photodecomposition; the RhB degradation % was calculated by the below formulae.

$$\text{Photo Degradation } \% = \left(1 - \frac{\text{At}}{\text{A0}}\right) * 100 \qquad \rightarrow \qquad \text{Equation 1}$$

Where A_0 is the absorbance of RhB at an initial time and A_t is the absorbance of RhB at a time ‘t’ during the degradation process.

2.6. Analysis of hydroxyl radical

Hydroxyl radicals (•OH) are extremely reactive species which are mainly responsible for photocatalytic degradation of dye molecules. The PL technique is used to identify the hydroxyl radical (•OH) formation using Terephthalic acid (TPA) as an ideal molecule on the surface of NTG5 photocatalyst. Highly fluorescent 2-hydroxyterephthalic acid (TAOH) was attained by the rapid reaction of TPA with photoinduced •OH and found around at 420 nm wavelength [29]. The most favorable concentration of Terephthalic acid solution was about 5×10^{-4} M in a diluted 2×10^{-3} M NaOH aqueous solution. A similar experimental process was followed to detect hydroxyl radical’s generation as, like photocatalytic decomposition of dyes, the TPA solution was taken instead of dye solution. Taken solution after 30 min of irradiation interval and centrifuged, that TAOH clear solution was examined by calculating absorbance at its excitation wavelength of 315 nm using Hitachi F-7000 fluorescence spectrophotometer.

3. Results And Discussion

3.1 XRD analysis

As shown in Fig. 2a, XRD analysis of various samples such as graphite, synthesized GO, and NTG composites were carried out. The diffraction peak centered at $2\theta = 26.19^0$ was found a clear (002) orientation of pure graphite with an interlayer spacing of 0.34 nm is depicted in Fig. 2a. The degree of oxidation in XRD is directly proportional to the spacing between the interlayers of the materials. The formation of GO was confirmed by the appearance of the new peak at $2\theta = 12.68^0$ with an interlayer distance of 0.699 nm corresponding to the (002) lattice plane. It is well known that owing to the oxygen-containing functional group's deposition on the graphene surface and disruption of the ordering of graphene sheets in graphite [26].

Out of the different crystalline forms available for TiO_2, the anatase form of TiO_2 is best suitable for a combination of photoactivity and photostability [30]. Comparison of XRD results of pristine TiO_2 with that of the NT and NTG composites reveals that all diffraction patterns essentially identical as evident from Fig. 2b. All the discerned peaks for NTG nanocomposites at $2\theta = 25.06^0$, 37.27^0, 47.99^0, 54.8^0, 62.32^0, 68.8^0 can be signed to the respective anatase crystal faces of (101), (004), (200), (211), (204) and (220) which is in well concord with the JCPDS No. 21-1272. The relevant peaks for rutile and brookite phases are absent which are usually appeared at $2\theta = 27.3^0$ and $2\theta = 30.8^0$ in all XRD patterns of NTG composites implying that formation of pure anatase TiO_2 at low temperatures. It also suggested that the absence of reflections from impurity phases, i.e., from Nb_2O_5 or NbO_2, proper doping of Nb into TiO_2 lattice occurred. Moreover, it can be identified that reappearance of the (002) diffraction line and no sign for the peak at 12.68^0 in XRD patterns referred that GO has been reduced to rGO and as such restored the ordered crystal structure. There is no significant peak relevant to rGO observed in composites, possibly due to the comparatively low concentration of GO in the composites capped by the strong (101) diffraction signal from crystalline TiO_2. Furthermore, the existence of rGO in NTG5 nanocomposites explained clearly in Raman analysis.

In addition, it is noticed that the slight broadening in peak width with the introduction of GO (Fig. 2b) occurred. It can be viewed from Table 1 that the average crystalline size of NTG composites is smaller than that of pristine TiO_2 and NT which are estimated by using Debye-Scherrer's formula with respect to anatase peak. It is inferred that, because of the attained strong interactions between TiO_2 and graphene during the hydrolysis of sol samples, the TiO_2 crystalline particles were unable to agglomerate [31].

Table 1

Average crystallite size (nm), band gap energy (eV), BET surface area (m^2/g) and mean pore diameter (nm) of each catalyst.

S.No	Photocatalyst	Crystallite size (nm)	Band gap energy (eV)	BET surface area (m^2/g)	Mean pore diameter (nm)	Pore volume (cm^3/g)
1	NT	58.19	2.98	209.4	5.62	0.14
2	NTG1	30.73	2.68			
3	NTG5	29.58	2.62	256.5	4.24	0.18
4	NTG10	31.72	2.52			

3.2. UV-vis/DRS analysis

For visible light and sunlight induced photocatalysis, it is necessary that the catalysts must absorb the broad region of light (400–800 nm). From Fig. 3a it is observed that a significant influence on optical absorption of NTG nanocomposites by varying in the GO loads. Meanwhile, for NTG nanocomposites a red shift towards higher wavelength with strong and broad absorptions in the visible region can be distinctly detected indicates band gap narrowing of TiO_2 [32]. Besides, TiO_2 and NT spectrums are showing relatively lower absorption intensity compared with NTG nanocomposites in the visible region.

The optical band gap of photocatalysts is calculated using the Tauc's relationship. The Equation for band gap energy is described as below,

$$\sqrt{\alpha h\upsilon} = C(h\upsilon - Eg) \qquad \rightarrow \qquad \text{Equation 2}$$

where, h is Planck's constant, □ is the frequency of light, C is the proportionality constant, α is the absorption coefficient at a certain wavelength λ of the solid, E_g is the band gap energy.

Figure 3b displays the relationship between $(\alpha h□)^{1/2}$ and photon energy (h□=1239/λ) for TiO_2, NT and NTG nanocomposites. 2.98 eV is the band gap for NT, whereas the band gap of NTG nanocomposites is 2.68 eV, 2.62 eV and 2.52 eV correspond to NTG1, NTG5 and NTG10 respectively i.e., band gap energy decreases with increase in GO content. These results evident (listed in Table 1) that compare to the bare TiO_2 and NT, red shift was quantitatively observed in NTG nanocomposites. In general, functional groups with oxygen like epoxide, hydroxyl and carbonyl groups in GO are covalently attached to its sheet surfaces. The interactions between π electrons of GO and the existed surface free electrons of NT are accountable for the formation of the Ti-O-C bond structure, which subsequently causing in the shifting of the valence band and band gap energy reduction of nanocomposites [32]. These interactions can stimulate the photogenerated charge transfer from TiO_2 to GO and vice versa which subsequently leads to photocatalytic degradation enhancement of catalyst.

3.3. SEM and TEM analyses

Surface topography of produced photocatalysts was enlightened from SEM micrographs and surface modification as well as particle sizes were obtained by TEM analysis. The resultant SEM, TEM and HRTEM images for GO and NTG5 nanocomposite are depicted in Fig. 4. From SEM image of typical GO displayed in Fig. 4a, graphene sheets were observed which was implied by the presence of kinked and wrinkled shaped structures that were corrugated and scrolled intrinsic to graphene sheets [33]. Figure 4b presents the representative view of exfoliated GO, the observed crumples and folds in image suggested that the presence of typical single layered or multilayered GO. The existed functional groups on GO sheets could supports for nucleation and uniform growth of nanoparticles by providing reactive and anchoring sites [34]. It can be clearly identified from the TEM image (Fig. 4c) of NTG5 nanocomposite, it consists of a large amount of the spherically shaped NT nano particles (np's) that were uniformly anchored on rGO sheet surface without obvious agglomeration. Additionally, it also evident that NTG5 had the smallest particle size (approximately 5–10 nm) due to the hindering effects of rGO on the growth of NT np's. Taken together, the existed interaction between NT np's and rGO suggests that a complete conduction network could attain throughout the NTG5. This would allow injecting photogenerated electrons from NT np's into the rGO sheets upon which they are anchored and the electrons to flow through the graphene network within the composite rather than passing through the NT np's themselves. This could significantly cause enhancement in the photocatalytic efficiency of the photocatalyst. Figures 4d and 4e depict the HR-TEM images of NTG5 nanocomposite. These are unequivocal reveals that the specific interplanar spacing is 0.35 nm belonging to the (101) plane of anatase TiO_2, which are coincident with the results of XRD. The identification of crystalline fringes in rGO sheets is impossible due to the ultrathin structural network of rGO. From the SAED patterns of NTG5 (Fig. 4f), it was found that a typical 6-fold symmetric diffraction pattern observed in the NTG5 catalyst. Furthermore, the existence of the polycrystalline structure of TiO_2 in composites is matched with the XRD analysis results. Notably, any additional pattern in SAED corresponds to the crystalline impurities did not observed.

EDX spectrum of NTG5 (Fig. S1b) demonstrates that presence of Ti, O, and C mainly along with small quantities of dopant Nb which is significant to the successful generation of highly pure nanocomposite. Mainly, the signals for C and Ti could have emerged from the rGO sheets and the TiO_2 nanoparticles respectively. Following, the signal for O could be arisen from both TiO_2 and rGO because of its oxygen-containing functional groups. The elemental microanalysis of NT and NTG5 are summarized in Table S1.

3.4 BET analysis

Porous nature and surface area of photocatalyst were described by nitrogen adsorption-desorption measurement. The nitrogen sorption isotherms and distribution of pore sizes of NTG5 and NT np's can be found in Fig. 5. In accordance with the IUPAC representations, the microporous materials are having pore diameter smaller than 2 nm, substances having greater than 50 nm termed as macroporous materials; at last, substances lies in the middle fall under the mesoporous category and the isotherm of NTG5 nanocomposite shown in Fig. 5a corresponds to type IV classification and the type E hysteresis loop is an

exceptionally matched with the De Boer classification ascribed to the mesoporous solid substances [35]. The obtained BET specific surface area (S_{BET}) and pore volume (Vp) of NT and NTG5 are tabulated in Table 1. Significantly, the surface area of NTG5 (256.5 m^2/g) is greater than that of NT (209.4 m^2/g), it might be attributed due to the deposition of NT np's on the surface of rGO in NTG5 nanocomposite. This may be attained either because of the rGO sheets stacking structure or by the insertion of rGO layers that minimizes the NT np's agglomeration.

In addition, pore size distribution curves were plotted (shown as in Fig. 5b) which are calculated by the BJH (Barrett-Joyner-Halenda) method from the desorption isotherm. From the BJH plot of NTG5 nanocomposite, it can be understood that the majority of the pores lie below 10 nm and exhibits a peak at 3.32 nm denotes its mesoporous nature. Further, it is observed that the obtained average mean pore diameter of NTG5 and NT np's were 4.24 nm and 5.62 nm, respectively lies under mesoporous which are distributed uniformly. Thus, the smaller pore diameter in NTG5 reflects its smaller particle sizes, coincides with the SEM and TEM characterization results. Therefore, greater S_{BET} and pore volume of NTG5 nanocomposite can efficiently provide the enhanced absorption of dye molecules on its surface in aqueous solution which results in an enhancement in photocatalytic degradation of dye.

3.5. XPS analysis

Chemical states of constituent elements in the as-synthesized NTG5 sample have been illustrated by XPS analysis and obtained results are portrayed in Fig. 6. The signals correspond to the Ti, O, Nb and C species can be clearly identified from the full range spectrum of NTG5 (Fig. 6a). As seen in Fig. 6b, the Ti 2p core level spectrum demonstrates a single pair of binding energy peaks corresponds to Ti $2p_{3/2}$ and Ti $2p_{1/2}$ are centered at 459 eV and 465 eV, respectively, which clearly represents the Ti^{+4} state [36]. The core level XPS spectra of C 1s and O 1s provide explicit information regarding the oxygen functional groups present in the graphene skeleton of NTG5 catalyst. A typical binding energy peak ascribed at 531 eV in O 1s core level XPS spectrum (Fig. 6c) indicates to metallic oxides (Ti-OH) as well as the residual –COOH [37]. In addition, according to the attained C 1s core level spectra in Fig. 6d, the characteristic main peak observed at 284.6 eV is attributed to sp^2 carbon in rGO which represents C-C, C = C, and C-H bonds. A peak at the binding energy of 288.4 eV devoted to carboxyl carbon (O = C-O) and/or Ti-O-C group [35, 38, 39]. Further, this will confirm by the FT-IR results. As shown in Fig. 6e, Nb 3d peaks at 207.8 eV and 210.8 eV corresponding to the Nb $3d_{5/2}$ and Nb $3d_{3/2}$ respectively. The presence of doublet represents the oxidation state of Nb as Nb^{+5} [40]. Moreover, due to lower synthetic temperatures, there is no signal at 281 eV observed for C 1s spectra which clearly reveals that there is no carbon doping in TiO_2 lattice. It is further noticed that, an observed significant reduction in the intensities of C-O-C and C-OH signals of currently obtained C 1s spectra of NTG5 nanocomposite with previously reported C1s spectra of GO suggesting that, during reaction process the precursor GO undergone partial reduction to rGO [36, 41].

3.6. Raman spectroscopy analysis

Raman spectroscopy is a broadly used technique to know ordered and disordered crystal structural behaviour of the carbonaceous materials. The information furnished by deflection in intensities and shifts of Raman bands explains C-C bonds nature and defects. The chemical composition of NTG5 nanocomposite was determined by correlating its Raman spectra with those of bare TiO_2 and GO. As delineated in Fig. 7a, the Raman spectral response obtained at 402.5, 517.8 and 641.6 cm^{-1} were assigned to the B_{1g} (1), $A_{1g}B_{1g}$ (2) and E_g (2) modes of NTG5 composite matches with the anatase structure of TiO_2 respectively which are coincident with the earlier reports [42, 43]. There are two respective noticeable peaks observed at 1350.3 and 1600.25 cm^{-1} in the GO spectrum relevant to D and G bands. On the other hand, the NTG5 nanocomposite shows these characteristic bands at 1375.6 and 1611.9 cm^{-1} in accordingly. The D band is usually attributed to A_{1g} symmetry breathing mode of k-point photons which is described disordered carbon, its defects, and edges. The G band ascribes from E_{2g} mode, relating to sp^2-bonded carbon atoms ordered structure. The shifting in both above bands in the NTG5 composite compared to GO exhibited the presence of interactions between NT np's and rGO. It is worth noting that, a decrease in D/G intensity ratio was recognized for NTG5 photocatalyst (I_D/I_G=0.837) comparing with GO (I_D/I_G=0.874), implying that the reduction of functional groups with oxygen (hydroxyl and epoxy) and the restoration of sp^2-bonded carbons. Further, it is confirmed the occurrence of rGO in the NTG5 composite. In conclusion, the Raman spectra conveyed the existence of rGO and anatase TiO_2 in NTG5 nanocomposite which is matched with the obtained XRD results.

3.7. FT-IR analysis

Further, synthesized GO and NTG nanocomposites were investigated by using FT-IR spectroscopy in order to ascertain the extent of ionic interactions between GO and NT np's. And the results obtained for Graphite, GO and NTG5 nanocomposite are depicted in Fig. 7b. The presence of prominent peaks of oxygen-containing functional groups like C-O-C (ν_{C-O-C} at 1231 cm^{-1}), C-OH (ν_{C-OH} at 1384 cm^{-1}), and C = O carbonyl groups ($\nu_{C=O}$ at 1720 cm^{-1}) in GO spectra verified that successful synthesis of hydrophilic GO by the oxidation of graphite. The broad peak at ~ 3404 cm^{-1} appeared for both GO and NTG5 nanocomposite assigned to the C-OH groups stretching vibrations and intercalated water within graphene sheets. NT np's are covalently anchored on the surface of GO through these surface functional groups with oxygen. Vibration band appearing around 1631.9 cm^{-1} in NTG5 nanocomposite assigned to the C-C vibration of graphene sheets. Significant low frequency bands corresponding to Ti-O-Ti and Ti-O-C were found around 651.6 cm^{-1} and 762.1 cm^{-1} respectively [44]. Thus, the obtained broad peak for the composite at the low frequency region reflects the chemical interactions between NT np's and rGO which results from the combination of Ti-O-Ti and Ti-O-C vibrations.

It can be clearly understood from the spectra of GO and NTG5 composite that carbonyl (C = O) and epoxy (C-O-C) stretching peaks were faded away and identification of sharp peak for C-O band in NTG5 confirms the existence of rGO formed by the slight reduction of GO during synthesis. Lastly, these results offered the presence of interfacial linkage in NTG5 nanocomposite which leads to an extended lifetime of

photoinduced e^{-}-h^{+} pairs. Consequently, this helps to improve in photocatalytic efficiency of NTG5 composite.

3.8. PL study

The photoluminescence study of NTG5 nanocomposite is certainly useful to ascertain the formation of •OH radicals on its surface during the irradiation process. The •OH radicals were examined by recording the high fluorescent characteristic peak acquired from 2-hydroxyterephthalic acid (TAOH) which was triggered during the reactions between terephthalic acid (TPA) and •OH radicals. Fig. S2 in ESI shows the variation in the PL emission spectra of TAOH with time under visible light exposure. A linear increase in the fluorescence intensities over the irradiation time at 420 nm was observed. Further illustrates that the spectral intensity of the TAOH is increasing with an increase in •OH production in water which are matches to the accordance with the former reports [29]. It portrayed that minimizing the charge recombination of electron-hole pair can be attained with greater in the formation of •OH. Thus, the generation of •OH shows a considerable positive response on the efficiency of the photocatalyst. Higher photocatalytic activity of nanocomposites can be achieved with the faster generation of •OH.

4. Photocatalytic Degradation Study

The photocatalytic activity of NTG nanocomposites was assessed by the widely accepted photocatalytic degradation reaction of dye (Here RhB as a model pollutant) under visible light exposure. These results were compared by taking NT photocatalyst as a reference.

4.1. Adsorption study

Before commencing the photocatalytic degradation of RhB under visible light irradiation, the adsorption behaviour of nanocomposites determined by keeping the mixture of RhB aqueous solution and photocatalysts under dark stirring for 30 min. The extent of adsorption capacity of the photocatalyst was measured by recording absorbance of RhB dye at its characteristic wavelength 554 nm which is proportional to its concentration. Results obtained (displayed in Fig. S3), indicates that both the NTG nanocomposites and NT photocatalyst show considerable adsorption towards RhB. Increased adsorption of RhB in the dark (7%, 22%, 27% and 30% for NT, NTG1, NTG5, and NTG10 respectively) has been observed with increasing rGO concentration from 1 to 10 wt% in nanocomposites. Notably, 27% of RhB adsorbed on the NTG5 catalyst surface; in contrast, only 7% of RhB solution was adsorbed for NT catalyst. This improvement in adsorption for NTG5 nanocomposite is caused by the introduction of graphene because of its crumpled surface could provide a larger surface area and mesoporosity. This illustrates that enhancement in adsorption of RhB dye molecules on nanocomposites results from the dispersion of NT np's on the surface of graphene, this could have resulted from π-π conjugation between RhB and aromatic regions of rGO [45]. In addition, NT np's prevents aggregation of rGO sheets on themselves during the formation of nanocomposites and it will enhance the adsorption capability of nanocomposites further. Such an intensive absorptivity is favorable for photodegradation of RhB on photocatalysts surface.

4.2 Effect of GO concentration

The photocatalytic performances of as-prepared NT photocatalyst, NTG1, NTG5, and NTG10 nanocomposites were assessed by deploying them in the decomposition of RhB as a model pollutant under visible light to validate most suitable concentration of GO in the nanocomposite. Figure 8 describes that the photocatalytic decomposition curves of RhB with NT and NTG nanocomposites under the stimulation of visible light at ambient conditions. Evidently, NTG nanocomposites are exhibited better photodegradation performance than the controlled sample NT as shown in Fig. 8a due to the availability of more contact surface between NT np's and RhB dye molecules by the incorporation of rGO [46]. From the experimental results, it can be stated that the photocatalytic efficiency following increasing trend with the amount of incorporated graphene content in nanocomposites and after optimum concentration of graphene load efficiency was decreased. It is clearly established in the case of NTG10 after optimum concentration of rGO, the activity was decreased with the further increment in GO amount. The fact behind this may be that excessive rGO content in composite offers more opportunities for the collision of the photogenerated electron-hole pair which consequently encourages their recombination. Nevertheless, it also suppresses the contact surface between NT np's and RhB dye molecules resulting in lower photocatalytic performance [2, 47]. In particular, it was found that NTG5 photocatalyst with 5 wt% rGO content displays higher photocatalytic activity. Approximately 98% of RhB was degraded photocatalytically with the NTG5 catalyst in 90 min under visible light stimulation followed by 93% for NTG1, 92% for NTG10 and 79% for NT. From the UV-vis absorption changes of RhB during photocatalytic decomposition with NTG5 catalyst shown in Fig. 8b, it can be seen that the maximum adsorption observed at 554 nm decreased with the raising light exposure time which demonstrates that the photodegradation of RhB steadily. It was revealed from RhB absorption spectra that there is no indication of the generation of by-products after slight decomposition, which tells that the dye is degraded completely by the photocatalysts.

From the plots of the degradation rate versus the illumination time (Fig. 8c), straight lines can be fitted in the first part of the plots, allowing to estimate apparent pseudo first-order kinetic constants follow the order NTG5 > NTG1 > NTG10 > NT plotted in Fig. 8d and tabulated in Table 2 [48]. As the degradation reactions proceed, significant deflection in degradation reaction rates from the straight line was found implying that the existence of adsorbed intermediates and/or products of the complete degradation adsorbed on the surface of the photocatalysts affect process [49]. The obtained photocatalytic degradation results were compared with the previously reported results and tabulated in the Table 3.

Table 2
Pseudo first-order kinetic rate constant (k), regression coefficient (R^2) and % of degradation of different photocatalysts for RhB dye under visible light irradiation.

S. No	Photocatalyst	Rhodamine B		% of degradation
		$k \times 10^{-4}$ in min^{-1}	R^2	
1	NT	1.68	0.95	78.69
2	NTG1	3.03	0.96	93.03
3	NTG5	3.98	0.93	97.67
4	NTG10	2.58	0.91	92.2

Table 3
Comparative table for photocatalytic efficiency of NTG5 nanocomposite with the previously reported results.

S. No	Nanocatalyst	Dye pollutant	% of degradation	Degradation time (min)	Reference
1	Nb doped TiO_2 (under UV light irrdiation)	Rhodamine B	90.00	60	51
2	TiO_2-GO	Methyl Orange	35.00	180	52
3	CdS-graphene/TiO_2 composite	Methylene Blue	33.00	150	53
4	TiO_2/N-Graphene nanocomposite	Eosin Y	63.40	180	54
5	rGO/Ag/Fe-doped TiO_2	Methylene Blue	95.33	150	55
6	Nb doped TiO_2/rGO nanocomposite (5% GO)	Rhodamine B	98.00	90	Present study

4.3 Effect of catalyst dosage for NTG5 catalyst

To investigate the suitable catalyst concentration of NTG5 for RhB photocatalytic degradation, sequential experiments were conducted at identical conditions (RhB dye, 2 mg/L) by varying amounts of NTG5 photocatalyst from 0.025 g to 0.075 g in 100 mL of RhB dye solution. As shown in Fig. 9a, it is clearly described that the degradation rates have been increased slightly with the amount of catalyst up to 0.050 g and then suppresses with further increase. This was happened due to the following main reasons. Firstly, more number of catalyst active sites are becoming available with the increasing amount of the catalyst which helps to adsorb more RhB dye molecules as well as to absorb photons leading to the increase in photocatalytic behavior of catalyst. In addition, the solution turbidity increases with further

increase in higher proportions of catalyst even though more areas are available for RhB molecules for adsorption. This hinders the penetration of light through and also scatters the exposed radiation. Collision held between ground state molecules and activated molecules may also one more added cause for lesser photocatalytic efficiency [50]. Thus, the addition of catalyst above a certain level may not contribute to excess catalytic efficiency, hence degradation rate decreases.

4.4 Effect of dye concentration for NTG5 catalyst

The effect of RhB dye concentration on its photodegradation was deliberated by taking a fixed amount of NTG5 catalyst. From Fig. 9b, it has been illustrated that the degradation rate increases with the increase in dye concentration from 2 mg/L to 6 mg/L and a further increment leads to a decrease in degradation rate. This might be due to the quenching of active sites on the catalyst by absorption of more number of dye molecules on it which causes a decrease of the •OH radical generation on catalyst surface [50].

5. Recyclability And Stability Of Ntg5 Nanocomposite

The long-term viability of the photocatalyst for commercial applications mainly depends on the recyclability of the photocatalytic activity. In this experiment, the suspended solid (photocatalyst) in RhB dye suspension was collected from the reaction vessel and washed with Milli Q water followed by ethanol to examine the recyclability of as-synthesized NTG5 nanocomposite. Therefore, the same photocatalyst was utilized for five successive trials or runs in photocatalytic degradation of RhB dye solution under similar conditions repeatedly. After every 90 min of photocatalytic reaction, the concentration of the RhB was measured. The results clearly said that the NTG5 nanocomposite has great potential for the degradation up to five successive runs without significant loss in photocatalytic activity of the photocatalyst (Fig. 10). This slight depletion in photocatalytic activity may be due to the loss of the quantity of catalyst during washes and adhesion of dye molecules on the surface of the photocatalyst. After examination of the recyclability of tested nanocomposite, collected and checked it's stability by characterizing with XRD and FT-IR. The XRD and FT-IR patterns are similar even after five successive runs completed when compared with the prepared NTG5 nanocomposite (Fig. S4a and b). This indicates that the synthesized NTG5 nanocomposite is stable photocatalyst and reusable for successive five runs.

By considering all the above results, it was found that several factors play a significant role to achieve better photocatalytic efficiency of NTG5 nanocomposite under visible light irradiation. This includes adsorption capacity, light absorption behavior, and effective charge distribution ability through an interface of photocatalysts, which are explained below:

1) The larger surface area of catalyst helps to interact more number of dye molecules through aromatic regions of rGO on NTG nanocomposites [45, 46].

2) The existed Ti–O–C chemical bond at the interface between NT np's and rGO can narrow the band gap of TiO_2 and extends the photo-responding range [40].

3) Lengthening of e^{-}-h^{+} pair separation by electron insertion through existed interfacial chemical linkage (Ti-O-C), which greatly suppresses their combination e^{-}-h^{+} pair in the excited TiO_2 [31, 45].

During the photoreaction, the promotion of electron takes place from valence band to conduction band on the TiO_2 surface under visible light exposure. In the present catalyst system, dopant Niobium (Nb) can create a transitional energy state between the aforementioned two bands of TiO_2 which can effectively reduce the band gap energy of TiO_2. It is well-known that in semiconductor photocatalysis, charge recombination will occur rapidly. It is renowned that graphene can also generate e^{-}-h^{+} pairs under visible light exposure, these electrons from graphene surface can enter into the TiO_2 conduction band through π-π conjugation and vice versa. Further, the electron cloud on TiO_2 conduction band and rGO surface could produce hydroxyl radical (•OH) through superoxide formation by reaction with adsorbed oxygen on nanocomposites surface while the hole in the valence band also can generate •OH by reaction with water or OH^{-} that are absorbed on the surface of the catalyst. These generated •OH radicals are the most powerful tools to decompose the organic pollutants into CO_2, and H_2O. Based on the experimental results, a possible mechanism was proposed in an earlier reported publication from our group [27] as shown in Fig. 11.

Conclusions

The Nb doped TiO_2/rGO nanocomposites were successfully synthesized *via* in situ process by modified sol-gel method at room temperatures. The formation of the Nb doped TiO_2 nanoparticles and their incorporation on the rGO nanosheets surface was established by XRD, TEM, SEM, DRS, and EDX techniques. Furthermore, experimental results clearly recommended that there is a significant interaction between rGO and Nb doped TiO_2 nanoparticles. Thereafter, the influence of different operating factors such as GO concentration, catalyst loadings and dye concentration on photocatalytic degradation of RhB was demonstrated under light irradiation. These exercises confessed that GO concentration in Nb doped TiO_2 nanoparticles helps in the enhancement of RhB dye molecules adsorption in dark condition as well as observed an appreciable change in photodegradation efficiency was achieved compared with NT nanoparticles. The NTG5 exhibits greater photocatalytic efficiency towards RhB about 98% within 90 min among all the catalysts under visible light irradiation. Based on its excellent photocatalytic activity, stability and recyclability shows that NTG nanocomposites are promising materials for various practical applications in the field of photocatalysis and wastewater remediation.

Declarations

Availability of data and materials

All data generated or analyzed during this study are included in this published article [and its supplementary information files].

Competing interests

The authors declare that they have no competing interests

Funding

Not Applicable

Authors' contributions

NP planned the concept, carried out the experimental work, interpreted characterization and experimental results and written the original draft. TSR supervised the research work and written the original draft. IMR interpreted characterization and experimental results, assisted in original draft writing and review & editing of the manuscript. KVDL, GD, GJ and SAA were assisted in experimental work. All authors read and approved the final manuscript.

Acknowledgments

This work has been supported by the University Grants Commission, New Delhi, India for financial support in the form of JRF.

References

1. Bes-Pi´a A, Mendoza-Roca JA, Alcaina-Miranda MI, Iborra-Clar A, Iborra-Clar MI. Reuse of wastewater of the textile industry after its treatment with a combination of physicochemical treatment and membrane technologies. Desalination. 2002;149:169–74.
2. Tang C, Chen V. Nano filtration of textile wastewater for water reuse. Desalination. 2002;143(1):11–20.
3. Santhy K, Selvapathy P. Removal of reactive dyes from wastewater by adsorption on coir pith activated carbon. Bioresour Tech. 2006;97(11):1329–36.
4. Bokare AD, Chikate RC, Rode CV, Paknikar KM. Iron-nickel bimetallic nanoparticles for reductive degradation of azo dye Orange G in aqueous solution. Appl Catal B: Environ. 2002;79:270–8.
5. Robinson T, Mc Mullan G, Marchant R, Nigam. Remediation of dyes in textile effluent: a critical review on current treatment technologies with a proposed alternative. Bio Resource Tech. 2001;77:247–55.

6. Quiroz AC, Barrera-D´ıaz C, Roa-Morales G, Hern´andez PB, Romero R, Natividad R. Wastewater ozonation catalyzed by iron. Indust Eng Chem Res. 2011;50(5):2488–2494.
7. Vamathevan V, Amal R, Beydoun D, Low G, Mcevoy S. Photocatalytic oxidation of organics in water using pure and silver-modified titanium dioxide particles. J Photochem Photobiol A. 2002;148(1–3):233–45.
8. Leary R, Westwood A. Carbonaceous nano materials for the enhancement of TiO_2 Photocatalysis. Carbon. 2011;49(3):741–72.
9. Mulpuri RK, Tirukkovalluri SR, Imandi MR, Alim SA, Kapuganti VDL. Zinc and boron co-doped nanotitania with enhanced photocatalytic degradation of Acid Red 6A under visible light irradiation. Sustain Environ Res. 2019;29:29.
10. Miditana SR, Tirukkovalluri SR, Raju IM, Alim SA, Jaishree G, Chippada MLVP. Gemini surfactant assisted synthesis of mesoporous Mn/Mg bimetal doped TiO_2 nanomaterial: characterization and photocatalytic activity studies under visible light irradiation. Sustain Environ Res. 2021;31:6.
11. Padmaja JS, Rao TS, Lakshmi KVD, Raju IM. Fabrication of hetero-structured mesoporours TiO_2-$SrTiO_3$ nanocomposite in presence of Gemini surfactant: characterization and application in catalytic degradation of Acid Orange. J Environ Chem Eng. 2018;6:6457–67.
12. Chandra MR, Rao TS, Kim HS, Pammi SVN, Prabhakarrao N, Raju IM. Hybrid copper doped titania/polythiophene nanorods as efficient visible light-driven photocatalyst for degradation of organic pollutants. J Asian Ceram Soc. 2019;5(4):436–43.
13. Raju IM, Rao TS, Lakshmi KVD, Chandra MR, Padmaja JS, Divya G. Poly 3-Thenoic acid sensitized, Copper doped anatase/brookite TiO_2 nanohybrids for enhanced photocatalytic degradation of an organophosphorus pesticide. J Environ Chem Eng. 2019;7:103211.
14. Wang P, Han L, Zhu C, Zhai Y, Dong S. Aqueous-phase synthesis of Ag-TiO_2-reduced graphene oxide and Pt-TiO_2-reduced graphene oxide hybrid nanostructures and their catalytic properties. Nano Res. 2011;4(11):1153–62.
15. Wang WD, Serp P, Kalck P, Faria JL. Visible light photo degradation of phenol on MWNT-TiO_2 composite catalysts prepared by a modified sol–gel method. J Mol Catal A: Chem. 2005;235(1–2):194–9.
16. Yang J, Zhang X, Wang C, Sun P, Wang L, Xia B, et al. Solar photocatalytic activities of porous Nb-doped TiO_2 microspheres prepared by ultrasonic spray pyrolysis. Solid State Sci. 2012;14(1):139–44.
17. Choi WY, Termin A, Hoffmann MR. The role of metal-ion dopants in quantum-sized TiO_2-correlation between photo reactivity and charge–carrier recombination dynamics. J Phy Chem. 1994;98(51):13669–79.
18. Woan K, Pyrgiotakis G, Sigmund W. Photocatalytic Carbon-Nanotube–TiO_2 Composites. Adv Mater. 2009;21(21):2233–9.
19. Allen MJ, Tung VC, Kaner RB. Honeycomb Carbon: A Review of Graphene. Chem Rev 2010;110(1):132–45.

20. Eda G, Fanchini G, Chhowalla M. Large-area ultrathin films of reduced grapheme oxide as a transparent and flexible electronic material. Nature Nanotech. 2008;3(5):270–4.
21. Geim AK, Novoselov KS. The rise of grapheme. Nature Mater. 2007;6(3):183–91.
22. Stankovich S, Dikin DA, Piner RD, Kohlhaas KA, Kleinhammes A, Jia Y, et al. Synthesis of graphene-based nanosheets via chemical reduction of exfoliated graphite oxide. Carbon. 2007;45:1558–65.
23. Marcano DC, Kosynkin DV, Berlin JM, Sinitskii A, Sun ZZ, Slesarev A, et al. Improved synthesis of graphene oxide. ACS Nano. 2010;4(8):4806–14.
24. Liu ZH, Wang ZM, Yang XJ, Ooi K. Intercalation of organic ammonium ions into layered graphite oxide. Langmuir. 2002;18(12):4926–32.
25. Jain R, Mathur M, Sikarwar S, Mittal A. Removal of the hazardous dye Rhodamine B through photocatalytic and adsorption treatments. J Environ Manage. 2007;85(4):956–64.
26. Hummers WS, Offeman RE. Preparation of Graphitic Oxide. J Am Chem Soc 1958;80(6):1339.
27. Prabhakarrao N, Ravichandra M, Sivarao T. Synthesis of Zr doped TiO_2/reduced Graphene Oxide (rGO) nanocomposite material for efficient photocatalytic degradation of Eosin Blue dye under visible light irradiation. J Alloys Comp. 2017;694:596–606.
28. Su H, Huang YT, Chang YH, Zhai P, Hau NY, Cheung PCH, et al. The Synthesis of Nb-doped TiO_2 Nano particles for Improved-Performance dye sensitized Solar Cells. Electrochem Acta. 2015;182:230–7.
29. Yu Y, Xiang Q, Zhou M. Preparation, characterization and visible-light-driven photocatalytic activity of Fe-doped titania nanorods and first-principles study for electronic structures. Appl Catal B Environ. 2009;90:595–602.
30. Gaya UI, Abdullah AH. Heterogeneous photocatalytic degradation of organic contaminants over titanium dioxide: a review of fundamentals, progress and problems. J Photochem Photobiol C. 2008;9(1):1–12.
31. Zhang Y, Tang ZR, Fu X, Xu YJ. Engineering the unique 2D mat of graphene to achieve graphene-TiO_2 nanocomposite for photocatalytic selective transformation: what advantage does graphene have over its forebear carbon nanotube. ACS Nano.2011;5(9):7426–35.
32. Dai K, Lu L, Liu Q, Zhu G, Liua Q, Liua Z. Graphene oxide capturing surface fluorinated TiO_2 nanosheets for advanced photocatalysis and the reveal of synergism reinforce mechanism. Dalton Trans. 2014;43(5):2202–10.
33. Meyer JC, Geim AK, Katsnelson MI, Novoselov KS, Booth TJ, Roth S. The Structure of Suspended Graphene Sheets. Nature. 2007;446:60–3.
34. Wang H, Robinson JT, Diankov G, Dai H. Nanocrystal Growth on Graphene with Various Degrees of Oxidation. J Am Chem Soc. 2010;132(10):3270–1.
35. Sing KSW, Everett DH, Haul R, Moscou L, Pierotti RA, Rouquerol J, et al. Reporting physisorption data for gas/solid systems with special reference to the determination of surface area and porosity. Pure Appl Chem. 1985;57:603–19.

36. Cheng Y, Zhao Q, Li Y, Peng W, Zhang G, Zhang F, et al. Gold Nano particles Supported on Layered TiO_2–RGO Hybrid as an Enhanced and Recyclable Catalyst for Microwave-assisted Hydration Reaction. RSC Adv. 2016;6:76151–7.
37. Park G, Bartolome L, Lee KG, Lee SJ, Park TJ. One-step sono-chemical synthesis of a graphene oxide–manganese oxide nanocomposite for catalytic glycolysis of poly (ethylene terephthalate). Nanoscale. 2012; 4:3879–85.
38. Abdelsayed V, Moussa S, Hassan HM, Aluri HS, Collinson MM, El-Shall M.S. Photothermal deoxygenation of graphite oxide with laser excitation in solution and graphene-aided increase in water temperature. J Phys Chem Letters. 2010;1:2804–9.
39. Wang F, Zhang K. Physicochemical and photocatalytic activities of self-assembling TiO_2 nano particles on nano carbons surface. Current Appl Phy. 2012;12:346–52.
40. Romero R, Ramos-Barrado JR, Martin F, Leinen D. Nb_2O_5 thin films obtained by chemical spray pyrolysis. Surf Interface Anal. 2004;36:888–91.
41. Zhang XY, Li HP, Cui XL, Lin Y. Graphene/TiO_2 nanocomposites: synthesis, characterization and application in hydrogen evolution from water photocatalytic splitting. J Mater Chem. 2010;20(14):2801–6.
42. Li N, Liu G, Zhen C, Li F, Zhang L, Cheng HM. Battery Performance and Photocatalytic Activity of Mesoporous Anatase TiO_2 Nano spheres/Graphene Composites by Template-Free Self-Assembly. Adv Function Mater. 2011;21(9):1717–22.
43. Liu G, Yang HG, Wang X, Cheng L, Lu H, Wang L, et al. Enhanced Photoactivity of Oxygen-Deficient Anatase TiO_2 Sheets with Dominant {001}Facets. Phys Chem C. 2009;113:21784–8.
44. Zhang H, Lv X, Li Y, Wang Y, Li J. P25-Graphene Composite as a High Performance Photocatalyst. ACS Nano. 2009;4:380–6.
45. Pan X, Zhao Y, Liu S, Korzeniewski CL, Wang S, Fan Z. Comparing Graphene-Tio_2 Nano wire and Graphene-TiO_2 Nano particle Composite Photocatalysts. ACS Appl Mater Interfaces. 2012;4(8):3944–50.
46. Perera SD, Mariano RG, Vu K, Nour N, Seitz O, Chabal Y, et al. Hydrothermal Synthesis of Graphene-TiO_2 Nano tube Composites with Enhanced Photocatalytic Activity. ACS Catal. 2012;2(6):949–56.
47. Wang P, Zhan S, Xia Y, Ma S, Zhou Q, Li Y. The fundamental role and mechanism of reduced graphene oxide in rGO/Pt-TiO_2 nano composite for high-performance photocatalytic water splitting. Appl Catal B: Environ. 2017;207:335–46.
48. Kim SY, Lim TH, Chang TS, Shin CH, Photocatalysis of methylene blue on titanium dioxide nanoparticles synthesized by modified sol-hydrothermal process of $TiCl_4$. Catal Lett. 2007;117:112–8.
49. Eberl J, Kisch H, Visible light photo-oxidations in the presence of α-Bi_2O_3. Photochem Photobiol Sci. 2008;7(11):1400–6.

50. Daneshvar N, Salari D, Khataee AR. Photocatalytic degradation of azo dye acid red 14 in water: investigation of the effect of operational parameters. J Photochem Photobiol. 2003;157(1):111–6.
51. Wang H.Y, Chen J, Xiao FX, Zheng J, Liu B. Doping-induced structural evolution from rutile to anatase: formation of Nb-doped anatase TiO_2 nanosheets with high photocatalytic activity. J Mater Chem A. 2016;4(18):6926–32.
52. Chen C, Cai W, Long M, Zhou B, Wu Y, Wu D, Feng Y. Synthesis of Visible-Light Responsive Graphene Oxide/TiO_2 Composites with p/n Heterojunction. ACS Nano. 2010;4(11):6425–32.
53. Par CY, Kefayat U, Viram N, Ghosh T, Oh WC, Cho KY. Preparation of novel CdS-graphene/TiO_2 composites with high photocatalytic activity for methylene blue dye under visible light. Bulletin Mater Sci. 2013;36(5):869–76.
54. Liu Y, Pei F, Lu R, Xu S, Cao S. TiO_2/N-graphene nanocomposite via a facile in-situ hydrothermal sol–gel strategy for visible light photodegradation of eosin Y. Mater Res Bulletin. 2014;60:188–94.
55. Jaihindh DP, Chen CC, Fu YP. Reduced graphene oxide-supported Ag-loaded Fe-doped TiO_2 for the degradation mechanism of methylene blue and its electrochemical properties. RSC Adv. 2018;8(12):6488–501.

Figures

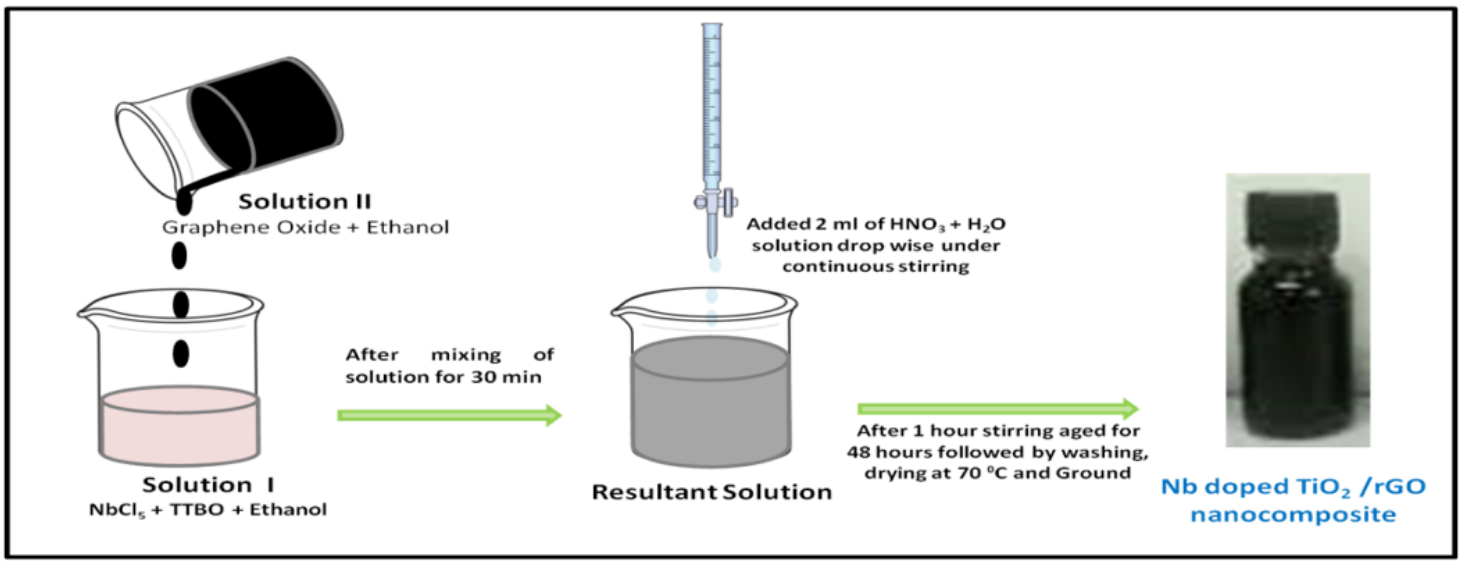

Figure 1

Schematic representation of synthesis of Nb doped TiO2/rGO nanocomposite.

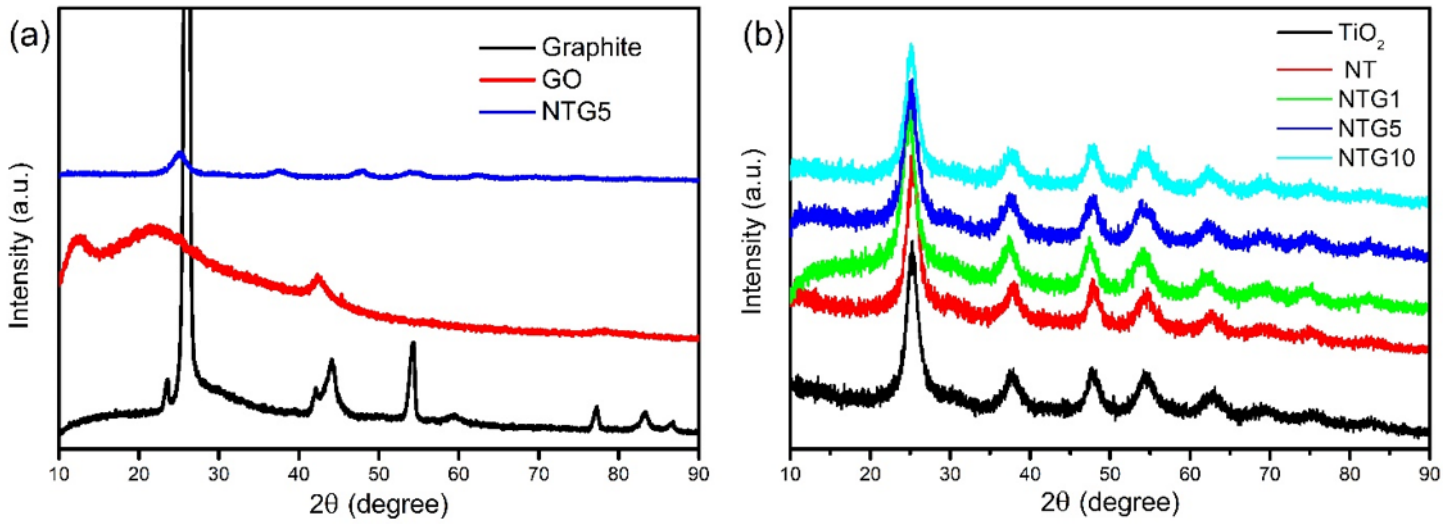

Figure 2

XRD patterns of Graphite, GO and NTG nanocomposites

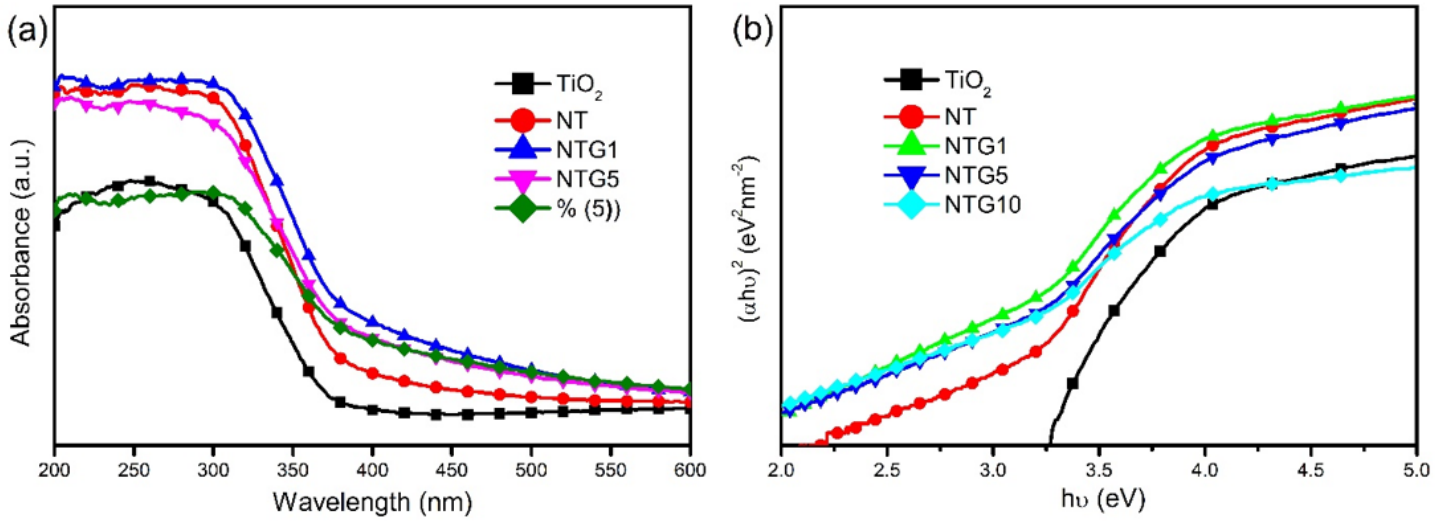

Figure 3

(a) The UV-vis diffuse reflectance absorption spectra and (b) corresponding Tauc's plot of NTG nanocomposites compared with NT.

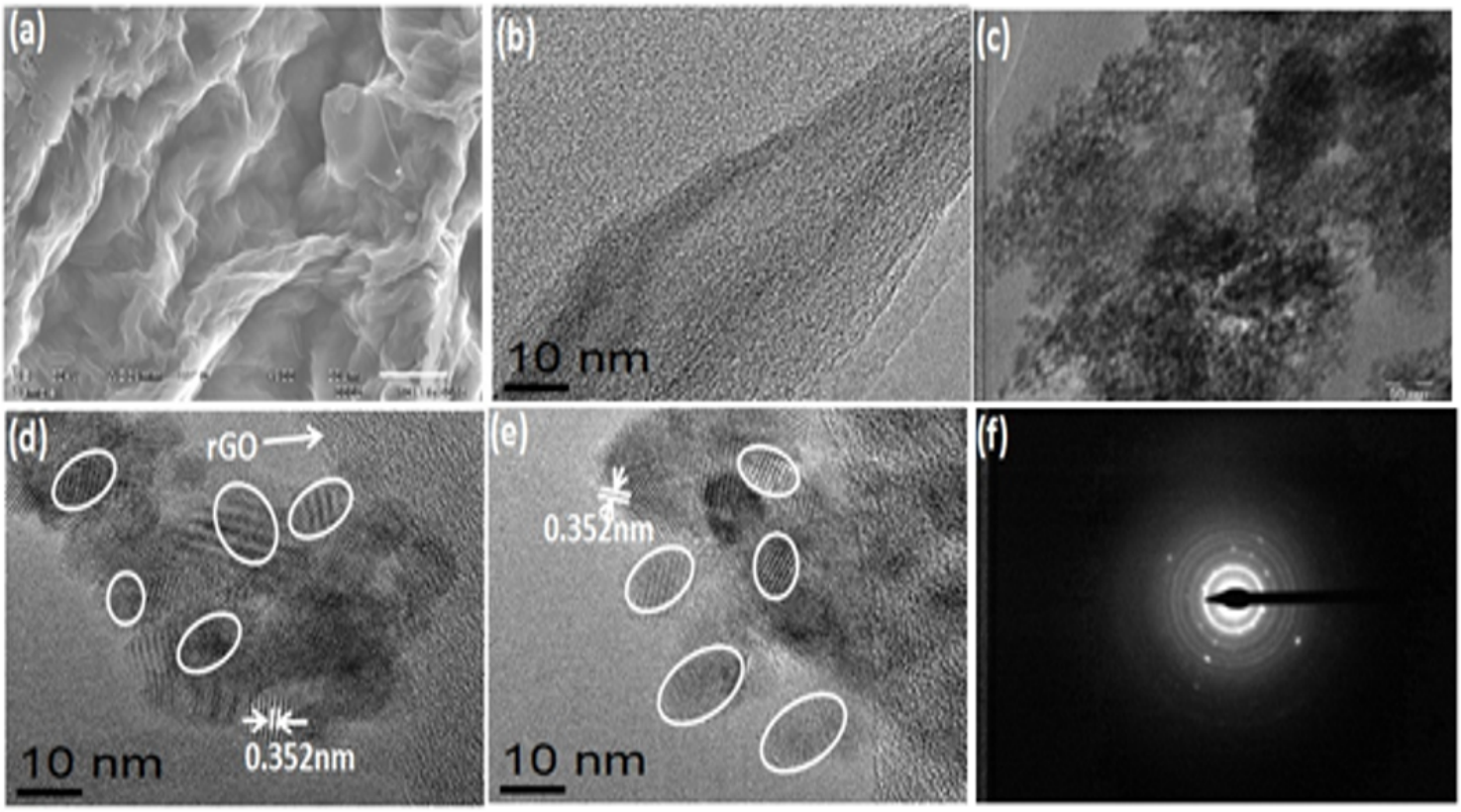

Figure 4

(a) SEM image of GO, (b) HRTEM images of GO, (c) TEM image of NTG5, (d) and (e) are HR-TEM images of NTG5, (f) SAED patterns of NTG5

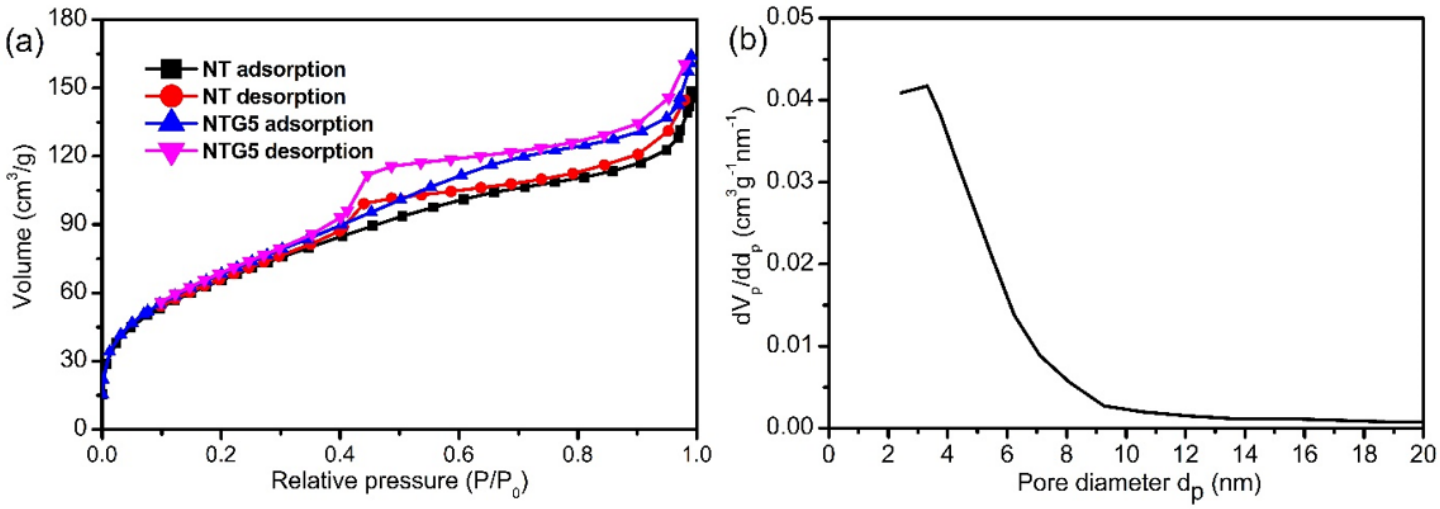

Figure 5

(a) Nitrogen adsorption-desorption isotherms of NT and NTG5 photocatalysts and (b) The corresponding BJH pore size distribution plot of NTG5

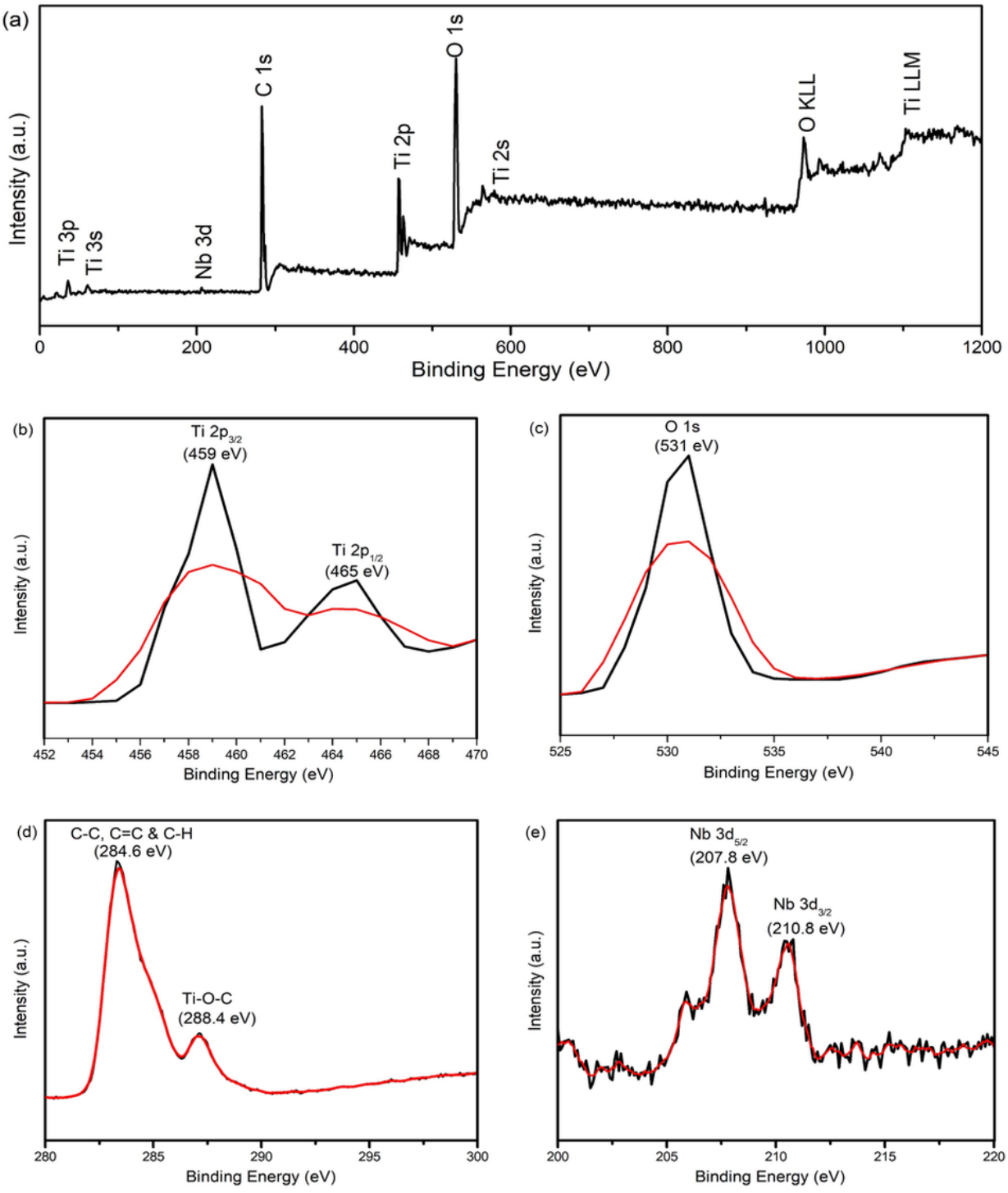

Figure 6

XPS spectra of NTG5 (a) Full range spectra, (b) Ti 2p spectra, (c) O 1s spectra, (d) C1s spectra and (e) Nb 3d spectra.

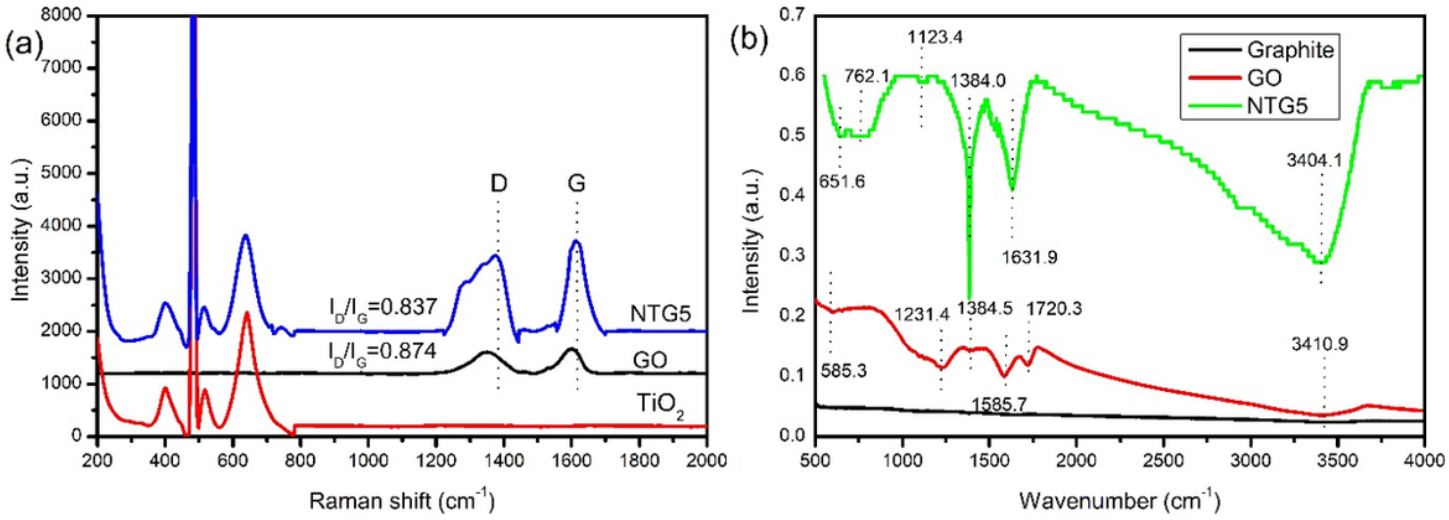

Figure 7

(a) Raman spectra of TiO2, GO and NTG5 (b) FT-IR spectra for Graphite, GO and NTG

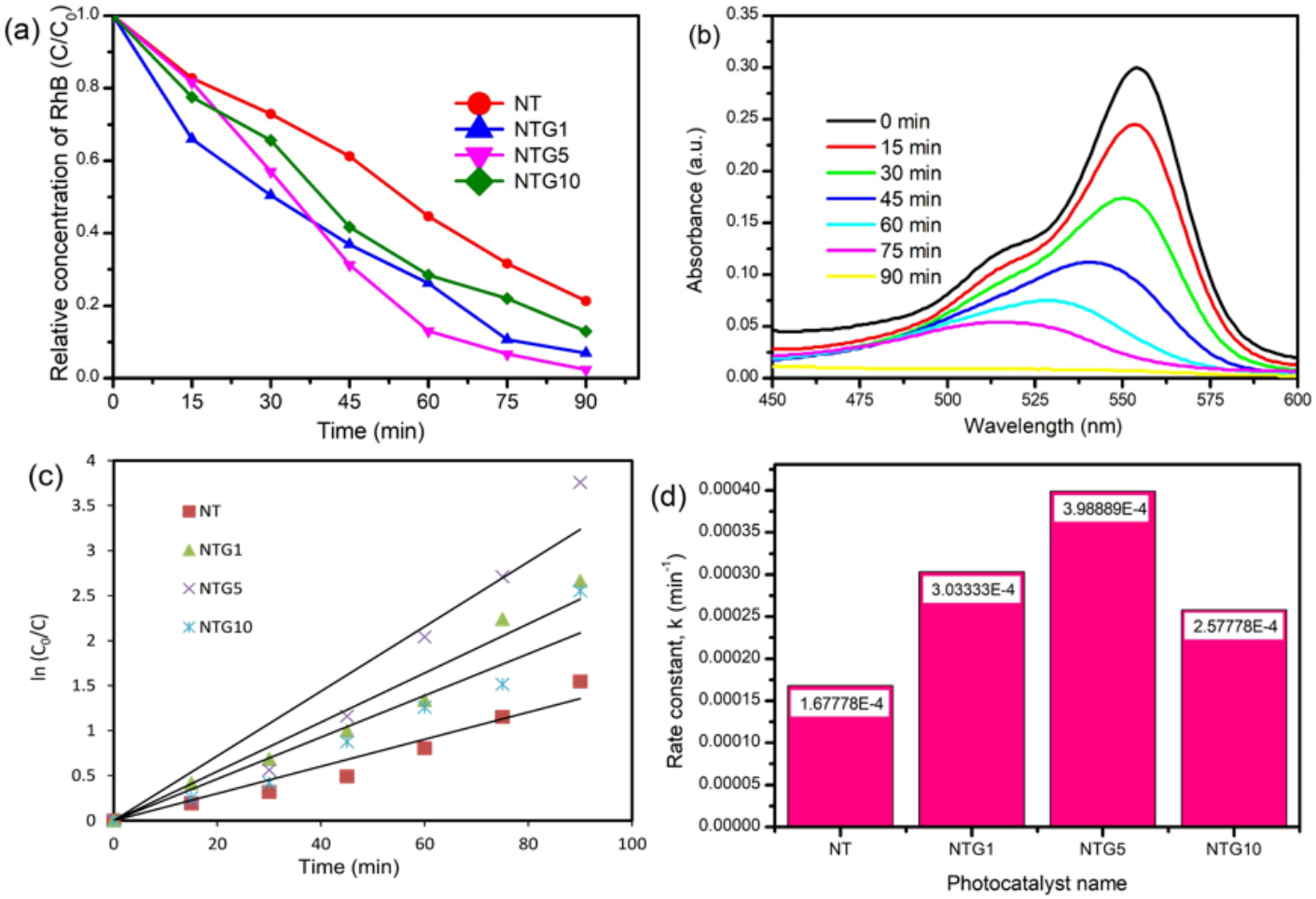

Figure 8

(a) Effect of rGO loads on the degradation of RhB dye by different photocatalysts, (b) UV-vis absorption spectra of RhB for NTG5 nanocomposite as a function of irradiation time, (c) Relation between irradiation

time and ln(c/c0) and (d) Pseudo first-order rate constants for photocatalytic degradation experiments of RhB with different photocatalysts.

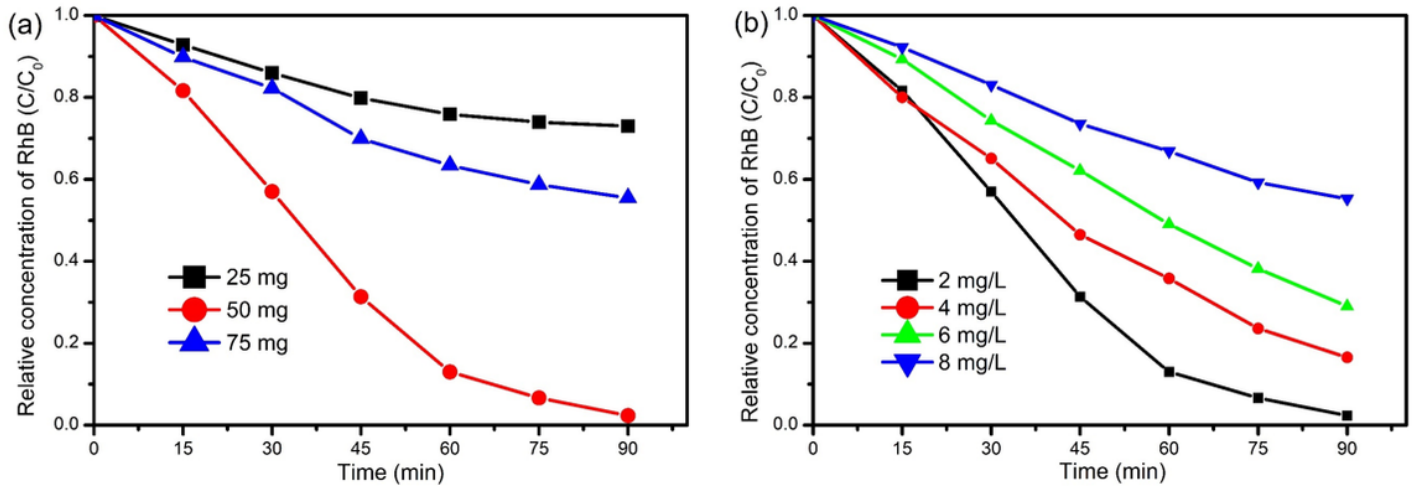

Figure 9

(a) Effect of catalyst dosage on photodegradation of RhB and (b) Effect of initial concentration of RhB on photodegradation.

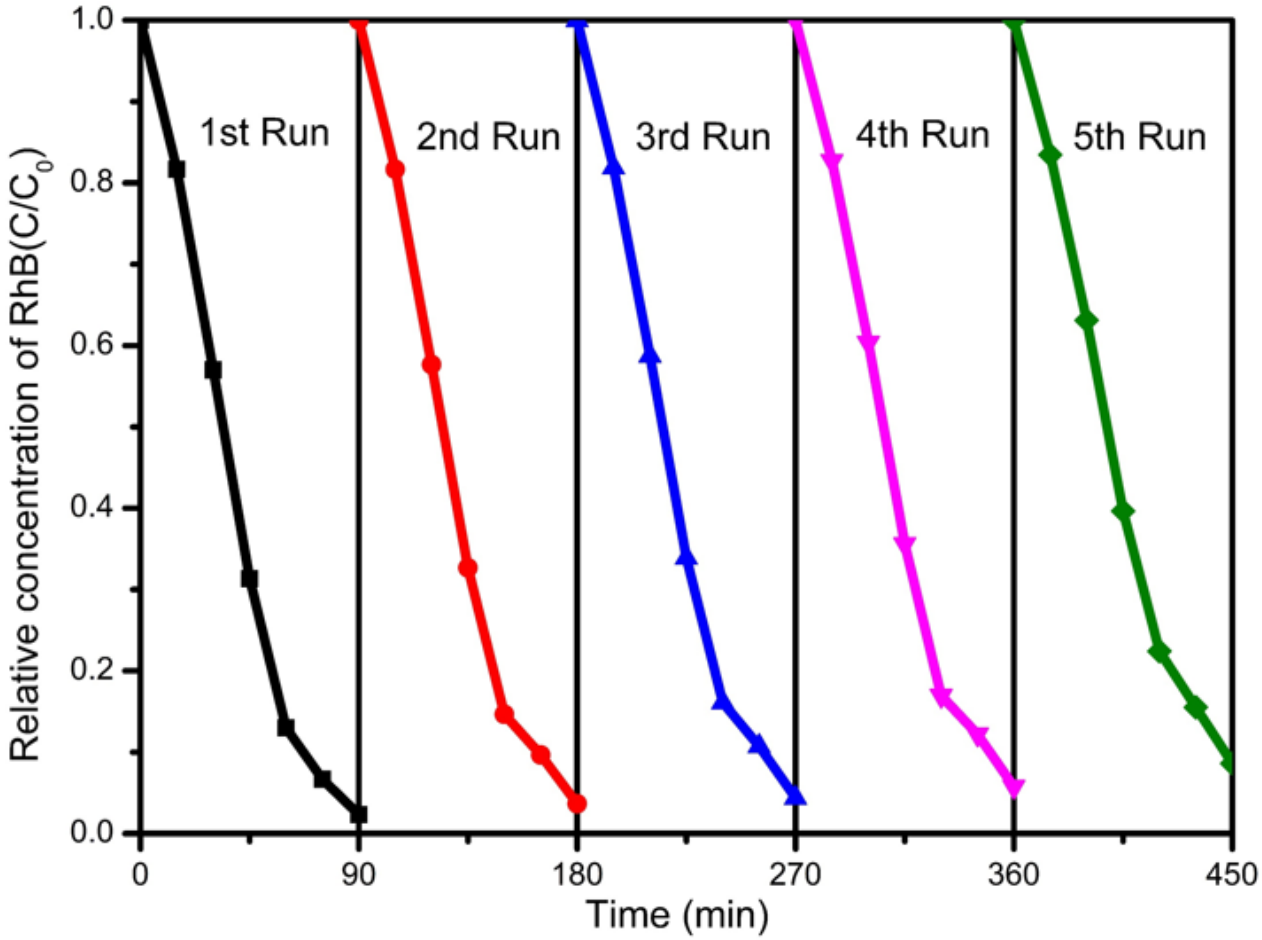

Figure 10

Recyclability test of NTG5 nanocomposite for consecutive reaction cycles

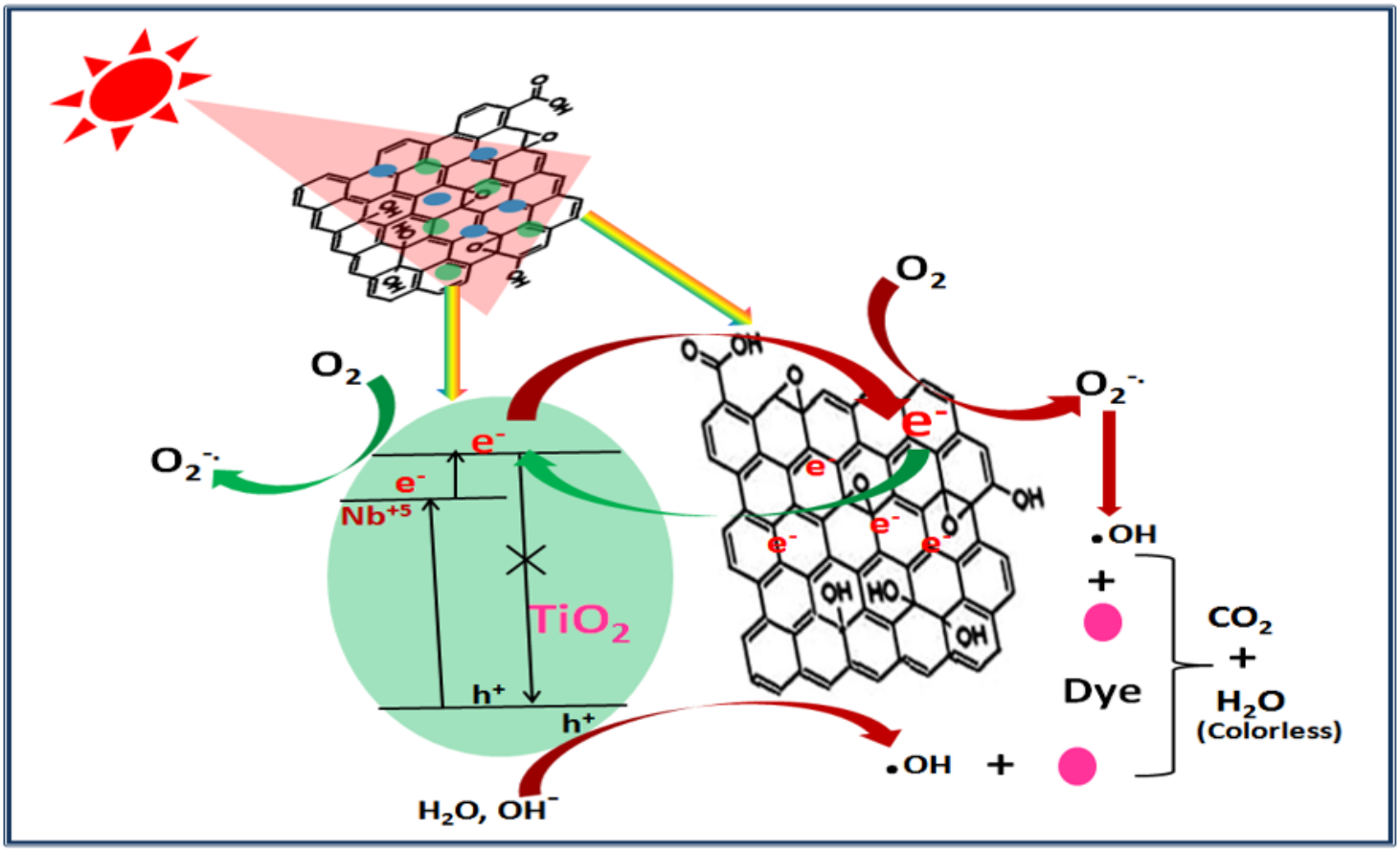

Figure 11

Schematic representation for degradation of RhB dye on Nb doped TiO2/rGO nanocomposites.

Supplementary Files

This is a list of supplementary files associated with this preprint. Click to download.

- SupplementaryMaterial.docx